APPENDIX B—MXER SIMULATION STUDY, PART II

STAR, Inc.

MXER SIMULATION STUDY

E. M. LEVIN

Part II

Prepared for MSFC
November 17, 2005

Typeset by AMS-TEX

NOMENCLATURE

A = first end-body
B = second end-body
C = center of mass of the tether system
E = longitudinal stiffness of the tether
$\mathbf{F}$ = non-gravitational forces
$\mathbf{g}$ = gravitational acceleration
J_C = moment of inertia of the tether system
L = total tether length
L_k = length of the k-th segment of the tether
m_A = mass of the first end-body
m_B = mass of the second end-body
m_k = embedded mass k
M = total mass of the tether system
$\mathbf{R}$ = geocentric radius-vector
R_E = mean radius of the Earth
R_C = geocentric radius of the center of mass
s = arclength along the unstretched tether
T = tether tension
$\mathbf{T}$ = tether tension vector
t = time
γ = tether elongation
ρ = tether mass per unit length
$\boldsymbol{\tau}$ = unit vector along the tether line
$\boldsymbol{\tau}_1$ = direction of the imaginary straight tether line
Ω = rotational angular rate
$(\dot{})$ = differentiation with respect to time
$(')$ = differentiation with respect to the arclength
$(\mathbf{a}, \mathbf{b})$ = scalar product of vectors $\mathbf{a}$ and $\mathbf{b}$

1. EQUATIONS OF MOTION IN NEWTONIAN FORM

In the first part of this study [1], we considered the dynamics of a momentum exchange system consisting of two end-bodies and a number of power stations connected with tether segments. The end-bodies A and B and the power stations k were modeled as point masses m_A, m_B, and m_k, respectively. The power stations are connected with tether segments of lengths L_k, as shown in Fig. 1. The tether segment L_k connects masses m_k and m_{k+1}.

Fig. 1. Structure of the momentum exchange tether system.

All point masses and the masses of the tether segments are assumed to be constant. Tether mass per unit length can vary along the tether.

Positions of the tether elements with respect to a non-rotating geocentric reference frame $OXYZ$ are defined by the geocentric radius $\mathbf{R}$ as a function of the arclength s measured along the unstretched tether from A to B, and time t,

$$\mathbf{R} = \mathbf{R}(s,t),$$

Positions of the end masses and embedded masses are

$$\mathbf{R}_A = \mathbf{R}(s_A,t), \quad \mathbf{R}_B = \mathbf{R}(s_B,t), \quad \mathbf{R}_k = \mathbf{R}(s_k,t).$$

The tension vector $\mathbf{T}$ of a perfectly flexible tether is tangent to the tether line,

$$\mathbf{T} = T\boldsymbol{\tau}, \qquad \boldsymbol{\tau} = \frac{\mathbf{R}'}{\gamma}, \qquad \gamma = |\mathbf{R}'|, \tag{1}$$

where $\boldsymbol{\tau}$ is a unit vector tangent to the tether line, prime denotes differentiation with respect to the arclength s, and γ is the local tether elongation.

The tether tension T can be expressed as a function of the elongation γ, elongation rate $\dot{\gamma}$, temperature Θ, and other factors,

$$T = T(s,\, t,\, \gamma,\, \dot{\gamma},\, \Theta, \ldots). \tag{2}$$

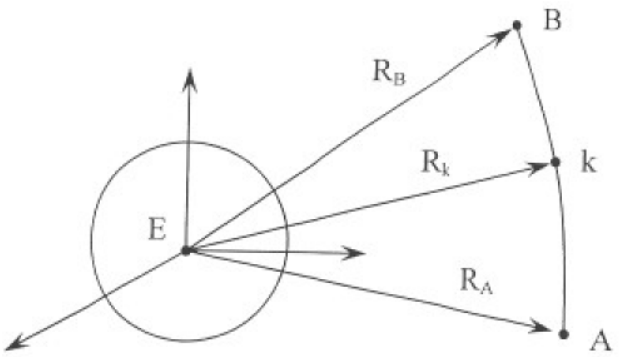

Fig. 2. Positions of the tether system elements.

Equations of motion of the tether system derived in [1] include ordinary and partial differential equations. The motion of the end masses and embedded masses is described by the ordinary differential equations

$$\begin{aligned} m_A \ddot{\mathbf{R}}_A &= \mathbf{T}_A + m_A \mathbf{g}_A + \mathbf{F}_A \\ m_B \ddot{\mathbf{R}}_B &= -\mathbf{T}_B + m_B \mathbf{g}_B + \mathbf{F}_B \\ m_k \ddot{\mathbf{R}}_k &= \mathbf{T}_{k+} - \mathbf{T}_{k-} + m_k \mathbf{g}_k + \mathbf{F}_k \end{aligned} \tag{3}$$

where dots denote differentiation with respect to time, $\mathbf{g}_A$, $\mathbf{g}_B$, and $\mathbf{g}_k$ are the gravity accelerations at points A, B, and k, respectively, while $\mathbf{F}_A$, $\mathbf{F}_B$, and $\mathbf{F}_k$ are non-gravitational forces acting on the end masses and embedded masses. The tether tension vectors are taken at the following points: $\mathbf{T}_A$ at point A, $\mathbf{T}_B$ at point B, $\mathbf{T}_{k-}$ at point k of segment L_{k-1}, and $\mathbf{T}_{k+}$ at point k of segment L_k.

The motion of the tether is described by the partial differential equation

$$\rho \ddot{\mathbf{R}} = \mathbf{T}' + \rho \mathbf{g} + \mathbf{F} \tag{4}$$

where dots denote differentiation with respect to time t, and primes denote differentiation with respect to the arclength s, ρ is the tether mass per unit length, and $\mathbf{T}$ is the tether tension.

In the general case, the tether mass per unit length ρ can vary along the tether, but we will concentrate on a more practical case when ρ is constant along each tether segment connecting the end masses,

$$\rho = \rho_k, \qquad k = 1, \ldots, K. \tag{5}$$

2. EQUATIONS OF MOTION IN MINAKOV'S FORM

Equations of motion in Minakov's form, introduced into space tether dynamics in [2], are obtained as follows. First, we differentiate equation (4) with respect to the arclength s,

$$\rho\,\ddot{\mathbf{R}}' = \mathbf{T}'' + \rho\,\mathbf{g}' + \mathbf{F}'.$$

Keeping in mind that $\mathbf{R}' = \gamma\tau$ and $\mathbf{T} = T\tau$, we find that

$$\rho\,(\ddot{\gamma}\tau + 2\dot{\gamma}\dot{\tau} + \gamma\ddot{\tau}) = T''\tau + 2T'\tau' + T\tau'' + \rho\,\mathbf{g}' + \mathbf{F}'. \tag{6}$$

By definition, the unit tangent vector τ satisfies the condition

$$(\tau,\tau) = 1. \tag{7}$$

The first differentiation with respect to the arclength and time yields two orthogonality conditions,

$$(\tau,\dot{\tau}) = 0, \qquad (\tau,\tau') = 0, \tag{8}$$

while the second differentiation yields two kinematic relations,

$$(\tau,\ddot{\tau}) = -(\dot{\tau},\dot{\tau}), \qquad (\tau,\tau'') = -(\tau',\tau'). \tag{9}$$

Multiplying equation (6) by vector τ (scalar product) and taking into account relations (7)–(9), we obtain a scalar equation of the second order with respect to tension,

$$\rho\,\ddot{\gamma} - \rho\gamma\,(\dot{\tau},\dot{\tau}) = T'' - T\,(\tau',\tau') + \rho\,(\mathbf{g}',\tau) + (\mathbf{F}',\tau). \tag{10}$$

From this equation, we express the second derivative of tension as

$$T'' = T\,(\tau',\tau') + \rho\,\ddot{\gamma} - \rho\gamma\,(\dot{\tau},\dot{\tau}) - \rho\,(\mathbf{g}',\tau) - (\mathbf{F}',\tau). \tag{11}$$

Substituting expression (11) into equation (6), we arrive at the following equation of the second order with respect to the unit tangent vector τ,

$$\rho\,[\gamma\ddot{\tau} + 2\dot{\gamma}\dot{\tau} + \gamma\tau\,(\dot{\tau},\dot{\tau})] = T\,[\tau'' + (\tau',\tau')\,\tau] + 2T'\tau' + \rho\mathbf{g}' + \mathbf{F}' - (\rho\mathbf{g}' + \mathbf{F}',\tau)\,\tau. \tag{12}$$

This equation describes transverse motion of the tether and it has an obvious wave structure with a transverse wave velocity equal to

$$v_t = \sqrt{\frac{T}{\rho\gamma}}. \tag{13}$$

Equation (10) describes longitudinal motion of the tether and it also has a wave structure. To reveal this structure, we consider a case of linear elasticity,

$$T = T_0 + E(\gamma - \gamma_*), \tag{14}$$

where T_0 is a reference tension, E is the tether longitudinal stiffness, and γ_* is the equilibrium elongation under the reference tension T_0. According to (14), and keeping in mind that γ_* may vary with time and temperature, we have

$$\ddot{\gamma} = \frac{\ddot{T}}{E} + \ddot{\gamma}_*.$$

After substituting this relation into equation (10), we can clearly see that this equation has a wave structure with a longitudinal wave velocity equal to

$$v_e = \sqrt{\frac{E}{\rho}}. \tag{15}$$

The longitudinal wave velocity (15) is much higher than the transverse wave velocity (13), and therefore, the system of equations (10) and (12) is stiff in the sense that equation (12) describes high frequency longitudinal oscillations, while equation (10) describes transverse oscillations of much lower frequencies. The advantage of Minakov's form of the equations lies in the separation of the high and low frequency wave structures in the tether dynamics equations.

In the Newtonian field,

$$\mathbf{g} = -\frac{\mu_E \mathbf{R}}{R^3},$$

the gravity gradient along the tether is calculated as

$$\mathbf{g}' = -\frac{\mu_E \mathbf{R}'}{R^3} + \frac{3\mu_E \mathbf{R}}{R^5}(\mathbf{R}, \mathbf{R}') = \frac{\mu_E \gamma}{R^3}[3\mathbf{e}_R(\mathbf{e}_R, \boldsymbol{\tau}) - \boldsymbol{\tau}], \tag{16}$$

where μ_E is the gravitational constant of the Earth, $\mathbf{e}_R = \mathbf{R}/R$ is a unit vector along the geocentric radius vector $\mathbf{R}$, and $\mathbf{R}' = \gamma\boldsymbol{\tau}$. The corresponding gravitational term in the equation of longitudinal motion (10) is reduced to

$$(\mathbf{g}', \boldsymbol{\tau}) = \frac{\mu_E \gamma}{R^3}[3(\mathbf{e}_R, \boldsymbol{\tau})^2 - 1], \tag{17}$$

while the respective gravitational term in the equation of transverse motion (12) takes the form

$$\mathbf{g}' - (\mathbf{g}', \boldsymbol{\tau})\boldsymbol{\tau} = \frac{\mu_E \gamma}{R^3} 3(\mathbf{e}_R, \boldsymbol{\tau})[\mathbf{e}_R - (\mathbf{e}_R, \boldsymbol{\tau})\boldsymbol{\tau}]. \tag{18}$$

3. BOUNDARY CONDITIONS

The equations of tether motion must be complemented with boundary conditions at the ends of each tether segment. To derive these boundary conditions, we express the accelerations of the end masses A and B and the embedded masses m_k from equation (3)

$$\ddot{\mathbf{R}}_A = \frac{\mathbf{T}_A + \mathbf{F}_A}{m_A} + \mathbf{g}_A,$$
$$\ddot{\mathbf{R}}_B = \frac{-\mathbf{T}_B + \mathbf{F}_B}{m_B} + \mathbf{g}_B,$$
$$\ddot{\mathbf{R}}_k = \frac{\mathbf{T}_{k+} - \mathbf{T}_{k-} + \mathbf{F}_k}{m_k} + \mathbf{g}_k,$$

and from equation (4) at the ends of the tether segments,

$$\ddot{\mathbf{R}}_A = \left(\frac{\mathbf{T}' + \mathbf{F}}{\rho}\right)_A + \mathbf{g}_A,$$
$$\ddot{\mathbf{R}}_B = \left(\frac{\mathbf{T}' + \mathbf{F}}{\rho}\right)_B + \mathbf{g}_B,$$
$$\ddot{\mathbf{R}}_k = \left(\frac{\mathbf{T}' + \mathbf{F}}{\rho}\right)_{k+} + \mathbf{g}_k = \left(\frac{\mathbf{T}' + \mathbf{F}}{\rho}\right)_{k-} + \mathbf{g}_k.$$

This yields the following boundary conditions

$$\begin{aligned} \mathbf{T}'|_A &= \mathbf{Q}_A, & \mathbf{T}'|_B &= \mathbf{Q}_B, \\ \mathbf{T}'|_{k-} &= \mathbf{Q}_{k-}, & \mathbf{T}'|_{k+} &= \mathbf{Q}_{k+}, \end{aligned} \tag{19}$$

where

$$\begin{aligned} \mathbf{Q}_A &= \frac{\rho_A}{m_A}(\mathbf{T}_A + \mathbf{F}_A) - \mathbf{F}|_A, \\ \mathbf{Q}_B &= \frac{\rho_B}{m_B}(-\mathbf{T}_B + \mathbf{F}_B) - \mathbf{F}|_B, \\ \mathbf{Q}_{k-} &= \frac{\rho_{k-}}{m_k}(\mathbf{T}_{k+} - \mathbf{T}_{k-} + \mathbf{F}_k) - \mathbf{F}|_{k-}, \\ \mathbf{Q}_{k+} &= \frac{\rho_{k+}}{m_k}(\mathbf{T}_{k+} - \mathbf{T}_{k-} + \mathbf{F}_k) - \mathbf{F}|_{k+}. \end{aligned} \tag{20}$$

Note that the gravitational accelerations canceled out and are not included in the boundary conditions.

Keeping in mind that $\mathbf{T}' = T'\boldsymbol{\tau} + T\boldsymbol{\tau}'$, according to (1), we multiply each of the relations (19) by the corresponding unit tangent vector $\boldsymbol{\tau}$ (scalar product) and arrive at the following conditions

$$\begin{aligned} T'|_A &= (\mathbf{Q}_A, \boldsymbol{\tau}_A), & T'|_B &= (\mathbf{Q}_B, \boldsymbol{\tau}_B), \\ T'|_{k-} &= (\mathbf{Q}_{k-}, \boldsymbol{\tau}_{k-}), & T'|_{k+} &= (\mathbf{Q}_{k+}, \boldsymbol{\tau}_{k+}), \end{aligned} \tag{21}$$

Relations (21) serve as boundary conditions for equation (10) describing longitudinal motion of the tether.

Substituting relations (21) into (19), we find boundary conditions for equation (12) describing transverse motion of the tether,

$$\begin{aligned} \boldsymbol{\tau}'|_A &= \frac{1}{T_A}\left[\mathbf{Q}_A - (\mathbf{Q}_A, \boldsymbol{\tau}_A)\,\boldsymbol{\tau}_A\right], \\ \boldsymbol{\tau}'|_B &= \frac{1}{T_B}\left[\mathbf{Q}_B - (\mathbf{Q}_B, \boldsymbol{\tau}_B)\,\boldsymbol{\tau}_B\right], \\ \boldsymbol{\tau}'|_{k-} &= \frac{1}{T_{k-}}\left[\mathbf{Q}_{k-} - (\mathbf{Q}_{k-}, \boldsymbol{\tau}_{k-})\,\boldsymbol{\tau}_{k-}\right], \\ \boldsymbol{\tau}'|_{k+} &= \frac{1}{T_{k+}}\left[\mathbf{Q}_{k+} - (\mathbf{Q}_{k+}, \boldsymbol{\tau}_{k+})\,\boldsymbol{\tau}_{k+}\right]. \end{aligned} \tag{22}$$

The boundary conditions are simplified when the non-gravitational forces $\mathbf{F}$ are neglected. The boundary conditions for the transverse motion of the tether are reduced to

$$\begin{aligned} \boldsymbol{\tau}'|_A &= \mathbf{0}, \\ \boldsymbol{\tau}'|_B &= \mathbf{0}, \\ \boldsymbol{\tau}'|_{k-} &= \frac{\rho_{k-}}{m_k}\,\frac{T_{k+}}{T_{k-}}\,(\boldsymbol{\tau}_{k+} - \varkappa_k \boldsymbol{\tau}_{k-}), \\ \boldsymbol{\tau}'|_{k+} &= \frac{\rho_{k+}}{m_k}\,\frac{T_{k-}}{T_{k+}}\,(\varkappa_k \boldsymbol{\tau}_{k+} - \boldsymbol{\tau}_{k-}), \end{aligned} \tag{23}$$

where

$$\varkappa_k = (\boldsymbol{\tau}_{k+}, \boldsymbol{\tau}_{k-}),$$

while the boundary conditions for the longitudinal motion of the tether take the form

$$\begin{aligned} T'|_A &= \frac{\rho_A}{m_A}\,T_A, & T'|_B &= -\frac{\rho_B}{m_B}\,T_B, \\ T'|_{k-} &= \frac{\rho_{k-}}{m_k}\,(\varkappa_k T_{k+} - T_{k-}), & T'|_{k+} &= \frac{\rho_{k+}}{m_k}\,(T_{k+} - \varkappa_k T_{k-}). \end{aligned} \tag{24}$$

4. MOTION OF THE CENTER OF MASS

The equations of tether motion derived in the previous sections describe evolution of the tether orientation and shape. They must be solved together with one of the ordinary differential equations (3) describing the orbital motion of one of the end masses or embedded masses, or with the equation of motion of the center of mass

$$\ddot{\mathbf{R}}_C = \frac{1}{M}(\mathbf{G}_0 + \mathbf{\Phi}_0), \tag{25}$$

where $\mathbf{R}_C$ is the geocentric radius vector of the center of mass, M is the total mass of the tether system, $\mathbf{G}_0$ is the sum of the gravitational forces

$$\mathbf{G}_0 = m_A\mathbf{g}_A + m_B\mathbf{g}_B + \sum_k m_k\mathbf{g}_k + \int_A^B \rho\mathbf{g}\,ds, \tag{26}$$

and $\mathbf{\Phi}_0$ is the sum of the non-gravitational forces acting on the tether system,

$$\mathbf{\Phi}_0 = \mathbf{F}_A + \mathbf{F}_B + \sum_k \mathbf{F}_k + \int_A^B \mathbf{F}\,ds. \tag{27}$$

As shown in the first part of this report [1], the sum of the gravitational forces can be represented as a series

$$\mathbf{G}_0 = M\mathbf{g}_C^0 + \sum_{n=2}^{\infty} \mathbf{g}_C^n I_n + \frac{\mathbf{\Phi}_0}{M}, \tag{28}$$

where $\mathbf{g}_C^0$ is the gravitational acceleration at the center of mass, $\mathbf{g}_C^n$ are derivatives of the gravitational acceleration along the "mean" tether line $\mathbf{R} = \mathbf{R}_C + (s - s_C)\,\tau_1$ drawn through the center of mass,

$$\mathbf{g}_C^n = \frac{1}{n!}\left.\frac{\partial^n \mathbf{g}}{\partial s^n}\right|_C,$$

and quantities I_n represent the high order moments

$$I_n = m_A(s_A - s_C)^n + m_B(s_B - s_C)^n + \sum_k m_k(s_k - s_C)^n + \int_A^B \rho(s - s_C)^n ds.$$

The direction of the "mean" tether line τ_1 is defined as follows. As shown in the first part of this report [1], the tether shape can be represented by the series

$$\mathbf{R}(s,t) = \mathbf{R}_C(t) + (s - s_C)\,\tau_1(t) + \sum_{n=2}^{\infty} \mathbf{q}_n(t)\,U_n(s), \tag{29}$$

where $\mathbf{q}_n(t)$ are generalized coordinates and $U_n(s)$ are the eigenforms of tether oscillations. Differentiating this equation with respect to the arclength, and keeping in mind that $\mathbf{R}' = \gamma\tau$, we derive

$$\tau_1 = \gamma\tau - \sum_{n=2}^{\infty} \mathbf{q}_n(t)\,U_n'(s). \tag{30}$$

The orthogonality conditions for the eigenforms can be expressed as

$$\int_A^B P\,U_i'U_j'\,ds = 0, \qquad i \neq j, \tag{31}$$

where $P = P(s)$ represents a normalized tension profile, defined as the solution to the following boundary problem [1],

$$\begin{aligned} P' &= -\rho\,(s - s_C), \\ P_A &= -m_A(s_A - s_C), \\ P_B &= m_B(s_B - s_C), \\ P_{k+} &= P_{k-} - m_k(s_k - s_C), \end{aligned} \tag{32}$$

The first eigenform describes the rigid rotation $U_1 = s - s_C$, for which $U_1' = 1$. Multiplying equation (30) by $PU_1' = P$, integrating over the entire tether length, and applying the orthogonality conditions (31), we find that

$$\tau_1 \int_A^B P\,ds = \int_A^B P\gamma\tau\,ds. \tag{33}$$

The integral of P, according to [1], is equal to the moment of inertia of the undeformed tether system about the center of mass

$$\begin{aligned} &\int_A^B P\,ds = ||U_1|| = J_C = \\ &m_A\,(s_A - s_C)^2 + m_B\,(s_B - s_C)^2 + \sum_k m_k\,(s_k - s_C)^2 + \int_A^B \rho\,(s - s_C)^2\,ds, \end{aligned} \tag{34}$$

and therefore, relation (33) can be rewritten as

$$\tau_1 = \frac{1}{J_C} \int_A^B P\gamma\tau \, ds. \tag{35}$$

Formula (35) defines the "mean" tether direction for any given tether shape under the assumptions of the current formulation.

Knowing τ_1, we can calculate derivatives (26). As shown in [1], the Newtonian term of the gravitational field gives

$$\mathbf{g}_C^n = -\frac{\mu_E \gamma_1^n}{R_C^{2+n}} \left[\mathbf{e}_R P'_{n+1}(x) + \mathbf{e}_1 P'_n(x) \right] \tag{36}$$

where $\mathbf{e}_R = \mathbf{R}_C/|\mathbf{R}_C|$ is the unit vector of the geocentric direction to the center of mass, $\gamma_1 = |\tau_1|$, $\mathbf{e}_1 = \tau_1/\gamma_1$, $P_n(x)$ are Legendre polynomials, and $x = -(\mathbf{e}_R, \mathbf{e}_1)$.

To close the system of equations, we need to find the geocentric positions of all elements of the tether system. For a given tether shape, we know the relative positions $\mathbf{r} = \mathbf{R} - \mathbf{R}_A$ of all elements, and from the definition of the center of mass, we can find its relative position

$$\mathbf{r}_C = \frac{1}{M}\Big(m_B \mathbf{r}_B + \sum_k m_k \mathbf{r}_k + \int_A^B \rho \, \mathbf{r} \, ds \Big). \tag{37}$$

Using this information, we can calculate the geocentric position of the end point $\mathbf{R}_A = \mathbf{R}_C - \mathbf{r}_C$ and the geocentric positions of all other points of the tether system $\mathbf{R} = \mathbf{R}_A + \mathbf{r}$.

5. QUASI-STATIC TENSION

The longitudinal oscillations of the tether system are directly affected by the internal friction in the tether, while the transverse oscillations are are affected indirectly, through a weak coupling with the longitudinal oscillations.

As discussed in [2], one way to model internal friction in the tether is to add a term $\rho\chi\dot{\gamma}$, where χ is an effective damping coefficient, to the left side of the equation of longitudinal motion (10). It is shown in [2] that the energy dissipation in the tether can rapidly damp out high frequency longitudinal oscillations, and after a short period of time the longitudinal motion becomes quasi-static. Tension variations in the quasi-static motion are induced by relatively slow transverse motions and can be described by equation (11) without the term $\rho\ddot{\gamma}$,

$$T'' = T(\tau', \tau') - \rho\gamma(\dot{\tau}, \dot{\tau}) - \rho(\mathbf{g}', \tau) - (\mathbf{F}', \tau). \tag{38}$$

At any given moment t, this equation can be treated as an ordinary differential equation with respect to the tether tension T. Along with the boundary conditions (21), it defines the tether tension profile as a function of the dynamic state of the tether, including the tether shape, elongation and the angular rate distribution along the tether.

Similar to (24), the boundary conditions (21) can be presented as

$$\begin{aligned} T'|_A &= \frac{\rho_A}{m_A} T_A + f_A, \\ T'|_B &= -\frac{\rho_B}{m_B} T_B + f_B, \\ T'|_{k-} &= \frac{\rho_{k-}}{m_k} (\varkappa_k T_{k+} - T_{k-}) + f_{k-}, \\ T'|_{k+} &= \frac{\rho_{k+}}{m_k} (T_{k+} - \varkappa_k T_{k-}) + f_{k+}, \end{aligned} \tag{39}$$

where

$$\begin{aligned} f_A &= \frac{\rho_A}{m_A} (\mathbf{F}_A, \tau_A) - (\mathbf{F}|_A, \tau_A), \\ f_B &= \frac{\rho_B}{m_B} (\mathbf{F}_B, \tau_B) - (\mathbf{F}|_B, \tau_B), \\ f_{k-} &= \frac{\rho_{k-}}{m_{k-}} (\mathbf{F}_k, \tau_{k-}) - (\mathbf{F}|_{k-}, \tau_{k-}), \\ f_{k+} &= \frac{\rho_{k+}}{m_{k+}} (\mathbf{F}_k, \tau_{k+}) - (\mathbf{F}|_{k+}, \tau_{k+}). \end{aligned}$$

As we see in relation (16), the gravity gradient $\mathbf{g}'$ calculated along the tether is proportional to the elongation γ, $\mathbf{g}' = \gamma \mathbf{g}'_0$. This is true for any gravitational field, not only Newtonian. Also, it has been shown in [2] that the aerodynamic and Ampere forces, as well as solar radiation pressure acting on a tether element are proportional to the elongation, $\mathbf{F} = \gamma \mathbf{F}_0$. Formally, the gradient of these forces $\mathbf{F}'$ will include quadratic terms in γ because of the variation of the environmental parameters along the tether, however, these terms can be linearized with respect to small variations of elongation.

Under these assumptions, if we use the linear elasticity relation (14) between the elongation and tension, then we will have

$$\gamma = \gamma_* + (T - T_0)/E, \tag{40}$$

and equation (38) will be linear with respect to T. The boundary conditions (39) will also be linear with respect to T.

The general solution of the linear boundary problem (38)–(39) at any given moment t can be represented as a sum of two solutions,

$$T(s,t) = T_0(s,t) + c_1 T_1(s,t). \tag{41}$$

Solution T_0 is obtained as follows. We set T_{0A} to zero and determine T'_{0A} from the first equation of the system (39),

$$T_{0A} = 0, \qquad T'_{0A} = f_A. \tag{42}$$

Then, we integrate equation (38) with the initial conditions (42) over the first tether segment and find T_{k-} and T'_{k-} at the end of the segment. Now, we use the third equation of the system (39) to find the tension at the beginning of the next tether segment

$$T_{k+} = \frac{1}{\varkappa_k}\left[T_{k-} + \frac{m_k}{\rho_{k-}}(T'_{k-} - f_{k-})\right]. \tag{43}$$

We then substitute quantity (43) into the last equation of the system (39) to find the derivative T'_{k+} at the beginning of the next segment.

This process is repeated until we arrive at the end B and determine the values of T_{0B} and T'_{0B}. Generally, these values will not satisfy the second equation of the system (39). We need solution T_1 to match the boundary condition at the end B.

Solution T_1 is calculated as follows. We introduce a new system of equations (38′)–(39′) which retains only terms linear in T from the original equations (38)–(39). We set T_{1A} to some reference tension T_*,

$$T_{1A} = T_*, \tag{44}$$

find T'_{1A} from the first equation of the homogeneous system (39′), and integrate the homogeneous equation (38′) over the first tether segment. We then use the third and the last equation of system (39′) to find T_{k+} and T'_{k+} at the beginning of the next segment, and continue integration until we reach the end B.

Now, we can substitute the general form of solution (41) into the second equation of (39) and find the coefficient c_1 from the following equation

$$T'_{0B} + \frac{\rho_B}{m_B}T_{0B} + c_1\left(T'_{1B} + \frac{\rho_B}{m_B}T_{1B}\right) = f_B. \tag{45}$$

One of the major benefits of this approach is that we reduced the initially stiff system of equations (10), (12) to a non-stiff system (12), (38) by abstracting from the fast transient processes in longitudinal oscillations. This does not mean that we neglected tether elongation, we only filtered out its high frequency components.

6. SIMULATION APPROACH

For a numerical solution, equations (12), (22), (38), (39) can be discretized with respect to the arclength s. This will reduce the partial differential equation

(12) to a set of ordinary differential equations at the discretization nodes. These equations are complemented with the ordinary differential equation (25) describing the motion of the center of mass.

The number of discretization nodes is determined by the required accuracy. To get an idea of a typical number of nodes, let us consider a very simple model of a string clamped at the ends A and B. Its transverse oscillations are decribed by the string equation

$$\rho\ddot{u} = Tu'',$$

where ρ is the string mass per unit length, T is the tension, assumed constant along the string, $u = u(s,t)$ is the transverse displacement, dots denote differentiation with respect to time t, and primes denote differentiation with respect to the arclength s.

The boundary conditions, are, obviously,

$$u_A = u_B = 0.$$

A discretized string equation looks as follows

$$\ddot{u} = v_t^2 \frac{u_{k+1} - 2u_k + u_{k-1}}{\Delta s^2},$$

where $v_t = \sqrt{T/\rho}$ is the transverse wave velocity, u_k is the transverse displacement at the node k, Δs is the distance between the neighboring nodes,

$$\Delta s = \frac{L}{N},$$

N is the number of nodes, and L is the length of the string.

Partial solutions representing the natural modes of oscillations are found in the form

$$u_k = \sin(\Omega_n t)\, \sin(\pi n \xi_k), \qquad n = 1, 2, \ldots$$

where Ω_n are the eigenfrequencies, and $\xi_k = k/N$, $k = 0, 1, \ldots, N$.

Substituting this form of solution into the discretized string equation, we find that the eigenfrequencies of the discretized problem are equal to

$$\Omega_n = 2N \frac{v_t}{L} \sin\left(\frac{\pi n}{2N}\right) \approx \pi n \frac{v_t}{L}\left(1 - \frac{\pi^2 n^2}{24N^2}\right).$$

The exact eigenefrequency obtained from the original partial differential equation is equal to

$$\Omega_n^* = \pi n \frac{v_t}{L}.$$

The relative difference is

$$\frac{\Omega_n - \Omega_n^*}{\Omega_n^*} \approx -\frac{1}{24}\left(\frac{\pi n}{N}\right)^2.$$

Because of the difference in eigenefrequencies, the phase difference between the simulated and exact solutions will accumulate with time as $\Delta\varphi = (\Omega_n - \Omega_n^*)t$. If we need to simulate the excitation of the n-th mode with a relative accuracy ε_n over a period of time Δt, then the difference between the eigenefrequencies must be limited as

$$|\Omega_n - \Omega_n^*| < \frac{\varepsilon_n}{\Delta t}.$$

To satisfy this relation, the number of nodes must be at least

$$N \gtrsim \pi n \sqrt{\frac{\pi n\, v_t \Delta t}{24 L\, \varepsilon_n}}.$$

For a typical momentum exchange system with $L = 90$ km and $v_t = 1$ km/s, it takes at least 125 nodes to maintain an accuracy of 1% for the first mode of transverse oscillations over one 3-hour orbit.

If an explicit integration scheme is used, then the time step will be limited by the condition of stability of the numerical solution. In general, this restriction has a form of

$$\Delta t < k_t \min_i \left\{\frac{\Delta s_i}{v_{ti}}\right\},$$

where k_t is a numeric coefficient depending on the implementation, Δs_i are the distances between the nodes, and v_{ti} are the maximum transverse wave velocities (13) between the corresponding nodes.

By comparison, in a lumped mass model, the time step is limited by

$$\Delta t < k_e \min_i \left\{\frac{\Delta s_i}{v_{ei}}\right\},$$

where k_e is a numeric coefficient depending on the implementation, and v_{ei} are the maximum longitudinal wave velocities (13) between the corresponding nodes.

The longitudinal wave velocity is much higher than the transverse wave velocity, and therefore the time step will be much smaller. This is why simulations based on the Minakov's form of the equations of motion are much faster than those based on lumped mass models.

Two numerical models were implemented, one using Minakov's form of the equations, and the other using a lumped mass model. With a sufficient number of nodes, as explained above, the results of the simulations were consistent between the models within the required accuracy. As expected, the Minakov's type model was by an order of magnitude faster than the lumped mass model.

7. RESONANT EXCITATION

It has been noted in simulations that the transverse oscillations of a typical momentum exchange system go through cycles of a long-term amplitude modulation, when the amplitude first builds up during a number of consecutive perigee passages, and then decreases again.

Fig. 3 shows a history of the transverse amplitude variations over the course of twelve orbits. The amplitude profile is shown in light gray, while the perigee passages are marked with black clusters underneath.

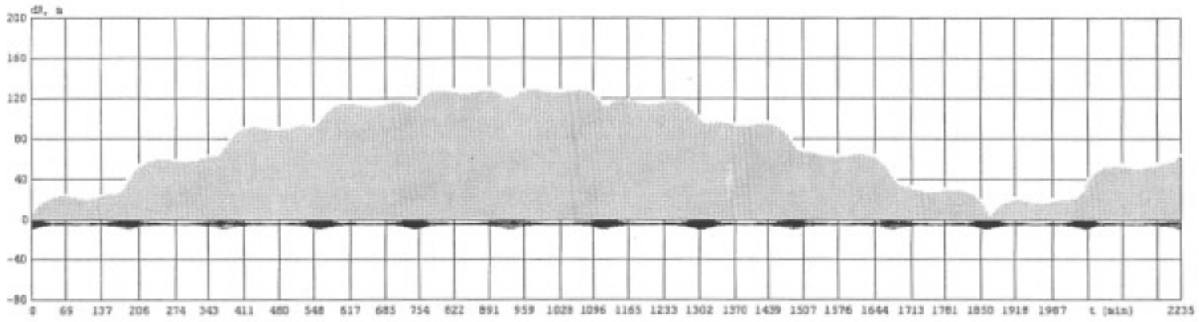

Fig. 3. Resonant excitation of the transverse oscillations.

We see that even without the initial excitation the amplitude of transverse oscillations steadily grows during five perigee passages until it reaches a relatively high level of over 120 m, stays at this level for another perigee passage, and then steadily decreases during the next five perigee passages. This cycle repeats with minor variations.

An in-depth analysis of this phenomenon based on the modal formulation developed in the first part of this report reveals that the mechanism of this excitation is resonant in nature and is caused by a sharp tuning between the natural frequency of the main mode of transverse oscillations U_2 and the frequency of the gravity gradient variation, which cycles twice per every rotation of the tether system about its center of mass.

This tuning is persistent in the sense that the parameters of the tether system must be changed radically to get away from the resonance. In particular, changing the spin rate has very little effect because the transverse frequencies are proportional to the spin rate, as shown in [1].

The modal formulation of Part I accurately describes the motion of the tether system in general and the resonant excitation of transverse oscillations in particular, when the term $\mathbf{Q}_n$ in the main modal equation (37) derived in Part I is used in its general form (38). The simplifications of the term $\mathbf{Q}_n$ demonstrated for a special case of an ideally tapered tether should remain restricted to this special case and should not be applied in case when the MXER tether is not carrying the full load for which it was designed.

For practical purposes, the modal solution requires very few modes and is computed much faster than the numeric solutions based on the Minakov's formulation, not to mention lumped mass models.

8. SENSITIVITY TO NON-GRAVITATIONAL PERTURBATIONS

8.1. Method of Computation.

To evaluate the sensitivity of the motion of the momentum exchange system to non-gravitational perturbations, we use the modal decomposition method described in Part I of this study [1].

As shown in [1], the effect of non-gravitational forces on the excitation of the eigenform U_n is determined by a generalized force

$$\mathbf{\Phi}_n = \mathbf{F}_A U_{nA} + \mathbf{F}_B U_{nB} + \sum_k \mathbf{F}_k U_{nk} + \int_A^B \mathbf{F}\, U_n\, ds. \tag{46}$$

It is computationally expensive to calculate the integral of $\mathbf{F}\, U_n$ over the entire tether length on each step. To make this calculation more efficient, we will use the following quadratic approximation on each tether segment $s_k \le s \le s_{k+1}$

$$\mathbf{F}(s,t) = (2\xi^2 - \xi)\,\mathbf{F}(s_k,t) + (1-4\xi^2)\,\mathbf{F}(s_{k+1/2},t) + (\xi + 2\xi^2)\,\mathbf{F}(s_{k+1},t), \tag{47}$$

where $\xi = (s - s_{k+1/2})/(s_{k+1} - s_k)$, and $s_{k+1/2} = (s_k + s_{k+1})/2$ is the middle of the segment, so that $-1/2 \le \xi \le 1/2$.

Using approximation (47), we have

$$\int_A^B \mathbf{F}\, U_n\, ds = \sum_k \mathbf{Q}_{nk}, \tag{48}$$

where

$$\mathbf{Q}_{nk} = \int_k^{k+1} \mathbf{F}\, U_n\, ds =$$
$$(2I^2_{nk} - I^1_{nk})\,\mathbf{F}(s_k,t) + (I^0_{nk} - 4I^2_{nk})\,\mathbf{F}(s_{k+1/2},t) + (I^1_{nk} + 2I^2_{nk})\,\mathbf{F}(s_{k+1},t),$$

and

$$I^0_{nk} = \int_k^{k+1} U_n ds, \qquad I^1_{nk} = \int_k^{k+1} U_n \xi \, ds, \qquad I^2_{nk} = \int_k^{k+1} U_n \xi^2 ds.$$

The coefficients I^m_{nk} can be precomputed before a simulation run, and to calculate the generalized forces (46), we would need to evaluate the environmental parameters only at the locations of the end masses and embedded masses and at the middle of each tether segment.

With typical parameters, the accuracy of this presentation of the generalized non-gravitational forces meets or exceeds precision requirements for modeling the dynamics of the momentum exchange system.

8.2. Aerodynamic Forces.

As shown in [2], the aerodynamic force acting on a tether segment can be approximated as

$$\mathbf{F} = -\rho_a d_t \gamma \left[|\tau \times \mathbf{v}_a| \left(\left(1 + \frac{\varepsilon}{3}\right) \mathbf{v}_a - \frac{4}{3} \varepsilon \mathbf{v}_\tau \right) + \nu (1 - \varepsilon) |\mathbf{v}_a| (\mathbf{v}_a - \mathbf{v}_\tau) \right], \qquad (49)$$

where d_t is the tether diameter, ρ_a is the air density, $\mathbf{v}_a$ is the tether velocity relative to the air, $\mathbf{v}_\tau = (\mathbf{v}_a, \tau)\tau$ is the component of the velocity $\mathbf{v}_a$ along the tether line, and ε and ν are small parameters, $0 < \varepsilon, \nu \lesssim 0.1$.

The aerodynamic forces acting on the end masses and the embedded masses are calculated as for regular satellites [4].

For a Hoytether [5] consisting of separate strands kept apart from each other, formula (49) must be applied to all individual strands. One must also take into account the overshadowing of the strands. In general, a Hoytether will have a larger total exposed area of the tether and a higher air drag.

With typical system parameters and Hoytethers having between 16 and 24 strands, it has been determined in numerical simulations that a 5% variation in the aerodynamics forces due to air density variations or uncertainties of the aerodynamic parameters of the tether will cause a 2 m shift of the tether tip A after one orbit.

8.3. Ampere Forces.

The Ampere force acting on a tether segment can be represented as

$$\mathbf{F} = I\gamma\tau \times \mathbf{B} \qquad (50)$$

where I is the electric current in the tether, and $\mathbf{B}$ is the geomagnetic induction vector.

Normally, Ampere forces should not be applied during a preparation for a rendezvous. However, to evaluate the sensitivity to the variations of the Ampere forces, we will consider a purely hypothetical situation when there is an electrical "leak" in the system, which results in a very small alternate electric current of a 1 mA amplitude flowing in the conductive segments of the tether in the direction of the EMF and modulated proportionally to the EMF. It was also assumed for simplicity that the "leak" current shuts off at altitudes above 2000 km for the lack of electrons.

It has been observed in simulations that this electric "leak" during the perigee passage causes a 3 m shift of the tether tip A after one orbit.

8.4. Solar Radiation Pressure.

The force of the solar radiation pressure acting on a round tether can be approximated as [2]

$$\mathbf{F} = -p_s d_t \gamma |\boldsymbol{\tau} \times \mathbf{e}_s| \left[\left(1 + \frac{\varkappa}{3}\right) \mathbf{e}_s - \frac{4}{3} \varkappa (\mathbf{e}_s, \boldsymbol{\tau}) \boldsymbol{\tau} \right], \tag{51}$$

where $\mathbf{e}_s$ is a unit vector of the direction to the Sun, p_s is the solar radiation pressure, and $\varkappa$ is the reflection factor.

The solar radiation pressure forces acting on the end masses and the embedded masses are calculated as for regular satellites [4].

For a Hoytether [5] consisting of separate strands kept apart from each other, formula (51) must be applied to all individual strands, taking into account their overshadowing. In general, a Hoytether will have a larger total exposed area of the tether.

With typical system parameters and Hoytethers having between 16 and 24 strands, it has been determined in numerical simulations that a 5% variation in the forces of solar radiation pressure due to uncertainties of the reflective and geometric parameters of the tether will cause a 1 to 4 m shift of the tether tip A after one orbit.

8.5. Thermal Expansion.

Thermal expansion changes the length of the tether segments and thus changes the moment of inertia of the momentum exchange system. The variations of the moment of inertia result in variations of the tether spin rate.

The moment of inertia is proportional to the second power of the average elongation γ_1, and in a simple case of a free rotation, when the angular momentum is conserved, the angular velocity Ω satisfies the relation

$$\gamma_1^2 \Omega = \gamma_0^2 \Omega_0. \tag{52}$$

When the average elongation γ_1 varies with the temperature Θ as

$$\gamma_1 = \gamma_0 + \alpha_t \Delta\Theta, \tag{53}$$

where α_t is the thermal expansion coefficient, then the angular rate will vary as

$$\Delta\Omega \approx -\frac{2\Delta\gamma_1}{\gamma_0}\,\Omega_0 = -\frac{2\alpha_t \Delta\Theta}{\gamma_0}\,\Omega_0.$$

If the average deviation of the actual temperature from the modeled temperature is $\Delta\Theta_{av}$ during a time Δt, then the angle of the tether in-plane orientation will deviate by $\Delta\vartheta = \Delta\Omega_{av}\Delta t$, and the transverse displacement of the tether end A will be estimated as

$$\Delta\vartheta\, L_{AC} \approx -\frac{2\alpha_t \Delta\Theta_{av}}{\gamma_0}\,\Omega_0 \Delta t\, L_{AC},$$

where L_{AC} is the distance from the end A to the center of mass C.

According to [3], Zylon, a candidate tether material, has a negative thermal expansion coefficient of $\alpha_t = -6 \times 10^{-6}$ 1/K. With a typical spin period of 6.3 min and a distance from the end to the mass center of 75 km, we find that after one orbital period of $\Delta t = 3$ hours, the tether end will drift away from its anticipated position by about 163 m per each Kelvin of the average temperature deviation. This sensitivity is attributed to the high spin rate Ω_0.

8.6. Creep.

The average elongation γ_1 will gradually increase with time due to creep,

$$\gamma_1 = \gamma_0 + \alpha_c \Delta t, \tag{54}$$

where α_c is the creep coefficient. In the approximation (52), the average spin rate will be dropping as

$$\Delta\Omega \approx -\frac{2\Delta\gamma_1}{\gamma_0}\,\Omega_0 = -\frac{2\alpha_c \Delta t}{\gamma_0}\,\Omega_0,$$

and the deviation of the angle of the tether in-plane orientation will be growing as

$$\Delta\vartheta \approx -\frac{\alpha_c (\Delta t)^2}{\gamma_0}\,\Omega_0.$$

The transverse displacement of the tether end A will build up with time as

$$\Delta\vartheta\, L_{AC} \approx -\frac{\alpha_c}{\gamma_0}\,\Omega_0 (\Delta t)^2\, L_{AC},$$

where L_{AC} is the distance from the end A to the center of mass C.

As reported in [3], the creep coefficient α_c of Zylon-HM under high stress is on the order of 10^{-6} 1/hour. For a 100-km tether, this will result in tether elongation at a rate of 2.4 m/day. With a typical spin period of 6.3 min and a distance from the end to the mass center of 75 km, we find that after one orbital period of $\Delta t = 3$ hours, the tether end will drift away from its anticipated position by about 41 m. For Zylon-AS, the creep coefficient and the tether end displacement are 3 times higher. As with thermal expansion, this sensitivity is attributed to the high spin rate Ω_0.

8.7. Mass Loss.

There are several processes that will contribute to the variation of the mass of the momentum exchange system:

(1) outgassing
(2) sublimation
(3) micrometeorite damage
(4) hollow cathode emission
(5) molecular deposition (mass addition)

While there is no reliable data on most of them, it has been estimated that a typical momentum exchange system may lose between 5 and 150 grams of its mass per day. As a result of this process, the center of mass of the tether system will be slowly shifting along the tether.

Let us consider the motion of a system with a straight, quasi-rigid tether, whose elements m_i are positioned at points s_i along the line

$$\mathbf{R}_i = \mathbf{R}_C + (s_i - s_C)\,\boldsymbol{\tau}, \tag{55}$$

where $\boldsymbol{\tau}$ is a unit vector, and subscript C refers to the center of mass. By the definition of the center of mass,

$$\sum_i m_i\,(s_i - s_C) = 0. \tag{56}$$

According to (56), when the masses of the elements m_i change, the center of mass slides along the tether at a rate of

$$\dot{s}_C = \frac{1}{M}\sum_i \dot{m}_i\,(s_i - s_C), \tag{57}$$

where M is the total mass of the tether system,

$$M = \sum_i m_i.$$

Differentiating (55) with respect to time, we obtain

$$\ddot{\mathbf{R}}_i = \ddot{\mathbf{R}}_C - \ddot{s}_C \boldsymbol{\tau} - 2\dot{s}_C \dot{\boldsymbol{\tau}} + (s_i - s_C)\ddot{\boldsymbol{\tau}}. \tag{58}$$

Multiplying (58) by m_i and performing summation, we find that

$$\sum_i m_i \ddot{\mathbf{R}}_i = M(\ddot{\mathbf{R}}_C - \ddot{s}_C \boldsymbol{\tau} - 2\dot{s}_C \dot{\boldsymbol{\tau}}), \tag{59}$$

where the terms with $\ddot{\boldsymbol{\tau}}$ canceled out because of the definition of the center of mass (56).

For each element of the system,

$$m_i \ddot{\mathbf{R}}_i = \mathbf{T}_i + \mathbf{F}_i + \mathbf{W}_i, \tag{60}$$

where $\mathbf{T}_i$, $\mathbf{F}_i$, and $\mathbf{W}_i$ are the sums of all internal, external, and reactive forces acting on this element. Substituting equations (60) for the individual elements into (59), we arrive at the following equation of motion of the center of mass

$$\ddot{\mathbf{R}}_C = \ddot{s}_C \boldsymbol{\tau} + 2\dot{s}_C \dot{\boldsymbol{\tau}} + \frac{1}{M} \sum_i (\mathbf{F}_i + \mathbf{W}_i). \tag{61}$$

All internal forces $\mathbf{T}_i$ cancel out after summation, as dictated by the Newton's third law. The terms with the derivatives of s_C describe the perturbation of the orbital motion because of the relocation of the center of mass.

Multiplying (58) by $\boldsymbol{\tau}$ (vector product) and performing summation, we find that

$$J_C \dot{\boldsymbol{\Omega}} = \sum_i (s_i - s_C)\boldsymbol{\tau} \times (\mathbf{F}_i + \mathbf{W}_i), \tag{62}$$

where J_C is the moment of inertia about the center of mass

$$J_C = \sum_i m_i (s_i - s_C)^2,$$

and $\boldsymbol{\Omega}$ is the angular velocity of the tether rotation

$$\boldsymbol{\Omega} = \boldsymbol{\tau} \times \dot{\boldsymbol{\tau}}.$$

It is interesting to note that even though the moment of inertia J_C is changing because of the mass loss, it does not directly result in the variation of the angular velocity, unlike the case of creep and thermal expansion.

While the hollow cathodes are expected to create a small torque of reactive forces $\mathbf{W}_i$, it is not obvious that the other processes involved in the mass exchange

with the environment will be anisotropic enough to create any noticeable torque of the reactive forces.

Assuming that the reactive torques are negligible, the gravitational field is Newtonian, and the non-gravitational forces are small, the in-plane perturbation of the orbit of the center of mass can be described, according to (61), as

$$\begin{aligned} \delta\ddot{x} - 2\omega\,\delta\dot{y} - \dot{\omega}\,\delta y - \left(\omega^2 + \frac{2\mu_E}{R_C^3}\right)\delta x &= \ddot{s}_C\cos\vartheta - 2\dot{s}_C\,\Omega\sin\vartheta, \\ \delta\ddot{y} + 2\omega\,\delta\dot{x} + \dot{\omega}\,\delta x - \left(\omega^2 - \frac{\mu_E}{R_C^3}\right)\delta y &= \ddot{s}_C\sin\vartheta + 2\dot{s}_C\,\Omega\cos\vartheta, \end{aligned} \tag{63}$$

where δx and δy are the vertical and horizontal displacements of the, center of mass, ω is the orbital angular rate, Ω is the spin rate, and ϑ is the angle between the tether and the local vertical. For a fast spinning tether, $\Omega \gg \omega$, we have $\vartheta \approx \Omega t$, and the order of magnitude of the perturbation is estimated as

$$\delta x^2 + \delta y^2 \sim \left(\frac{\ddot{s}_C}{\Omega^2}\right)^2 + \left(\frac{2\dot{s}_C}{\Omega}\right)^2.$$

These displacements are expected to be very small (less than a millimeter) because of the fast spin and slow shift of the center of mass.

9. ESTIMATION AND CONTROL REQUIREMENTS

As shown in the previous section, the position of the tether tip in the momentum exchange system is very sensitive to variations of the system and environmental parameters, when considered from the standpoint of the rendezvous precision requirements.

The variations producing the most impact on the tether tip positioning are related to the lengths of the tether segments, as we have seen in the case of thermal expansion and creep.

If the distances between the neighboring tethered modules could be measured with an accuracy of a few millimeters, then we could use this information to significantly improve the estimate of the current state of the momentum exchange system.

Every dynamic process in the momentum exchange system, one way or another, leaves its signature in the longitudinal motion of the tether. Using a detailed dynamic model, we may be able translate a continuous stream of precise distance measurements, combined with other data, into a reasonably accurate estimation of the tether system state.

Furthermore, using the information about the system state, we could compensate for some unexpected (or unmodeled) deviations from the projected path. In particular, deviations of the rotation about the center of mass could be corrected by slightly varying the tether length(s) or changing the mass distribution of the end bodies or power stations.

Given extremely short rendezvous windows with very fast relative motions, and various inherent uncertainties of the environment, it is very clear that elaborate estimation and control algorithms must be developed to make successful rendezvous with the momentum exchange system possible.

10. CONCLUSIONS

The task of prediction of the motion of a momentum exchange system with a 9-digit accuracy is extremely challenging, and it is relentlessly testing our ability to gain fundamental insights into the nature of the tether dynamics in this system.

It has been shown that the modal decomposition approach developed in the first part of this study is a very powerful and precise tool for the simulation of the dynamics of momentum exchange tethers.

However, to get a prediction with the required accuracy using this tool, one must have precise inputs, including the initial state, system parameters, and the environmental models. In simulations, the tether tip positioning has been observed to be quite sensitive to even small variations of the parameters involved in the calculations.

It is therefore imperative that precise estimation and control algorithms be developed to compensate for the inevitable uncertainties and support high precision rendezvous.

REFERENCES

1. LEVIN, E.M., MXER Simulation Study, Part I, MSFC Contract Report, January 10, 2005.
2. BELETSKY, V.V. AND LEVIN, E.M. Dynamics of Space Tether Systems. *Advances in the Astronautical Sciences,* AAS, **83,** 1993, Univelt, Inc.
3. PBO FIBER ZYLON, Technical Information, Toyobo Co., Ltd., Japan, 2001.
4. MONTENBRUCK, O. AND GILL, E. *Satellite Orbits: Models, Methods and Applications,* Springer Verlag, 2000.
5. HOYT, R.P., SLOSTAD, J.T. AND FRANK, S.S. A Modular Momentum-Exchange Electrodynamic-Reboost Tether System Architecture, AIAA-2003-5214, 2003.